JOURNAL OF GEOPHYSICAL RESEARCH, VOL. 104, NO. B3, PAGES 5047–5061, MARCH 10, 1999

Source of the climate signal recorded by magnetic susceptibility variations in Indian Ocean sediments

Mark W. Hounslow and Barbara A. Maher

School of Environmental Sciences, University of East Anglia, England, United Kingdom

Abstract. The origins of magnetic susceptibility variations in deep-sea sediments from the Indian Ocean (Ocean Drilling Program) (ODP Leg 117) have been examined to identify the specific connections between climate shifts and sediment magnetic properties. In a previous study, the magnetic susceptibility variations in ODP Hole 722B were identified as an outstanding proxy paleoceanographic record, despite evidence of postdepositional loss of magnetic minerals through reductive diagenesis. This paradox is addressed by assessing the contributions of ferrimagnetic detrital iron oxides, bacterial magnetosomes, and paramagnetic detrital Fe silicate minerals to the magnetic susceptibility signal. In addition to detailed magnetic analyses, mineralogical, morphological, and grain size data have been obtained from representative magnetic extracts. For Hole 722B, we find that magnetic responses to climate change result from (1) fluctuations in the volume magnetic susceptibility, which is primarily controlled by carbonate dilution; (2) a ferrimagnetic signal, which is restricted to the upper 7 meters below sea floor (mbsf) and which largely reflects source area aridity; and (3) a paramagnetic susceptibility record below 7 mbsf, which is coincident in frequency with variations in lithogenic grain size.

1. Introduction

Magnetic susceptibility records from sediments are widely used to provide a quantitative basis for correlation of sedimentary sequences and to identify missing or disturbed sediment sections. However, susceptibility records can have wider, indeed global, significance, as they can represent detailed proxy indicators of changes in paleoclimate and paleoenvironment, both in deep-sea cores [e.g., *Bloemendal*, 1983; *Robinson*, 1990; *Robinson et al.*, 1995] and in terrestrial sequences [e.g., *Heller et al.* 1993; *Maher et al.*, 1994]. Measurements of magnetic susceptibility can be made rapidly, easily, inexpensively, and nondestructively, thereby enabling compilation of high-resolution records. Shipboard logging of magnetic susceptibility is now routinely carried out on marine sediment cores, which reflects the scientific value of such measurements both for correlation and for deriving potential paleoclimatic information. However, to reconstruct paleoclimatic records from magnetic measurements, such as susceptibility, it is essential that the sources of the magnetic variations, and their specific linkages with climate, be identified, both on a site-specific basis and throughout the length of the sedimentary sequence at a site. Susceptibility variations within sediments can arise from changes in (1) the abundance and mineralogy of detrital magnetic minerals; (2) the abundance and mineralogy of magnetic material formed in situ, by authigenic processes; (3) the degree of preservation or dissolution of magnetic grains; and (4) the amount of diamagnetic biogenic material (carbonate and/or silica; for example, increased carbonate content will dilute the concentration of magnetic minerals).

The significance of each of these factors, which may vary both in time and space, is often primarily determined by climate, as is indicated by the frequent correlation between sediment magnetic properties and other climate indicators, such as the deep-sea oxygen isotope record. The aim of more detailed magnetic analyses, beyond simple measurements of magnetic susceptibility, is not merely to demonstrate or refine such correlations. Rather, we address the inverse problem: Can specific connections be identified between climate shifts and the measured sediment magnetic properties, thereby providing new and additional paleoclimatic information from these natural archives?

Here we examine the origins of magnetic susceptibility variations in deep-sea sediments that were recovered during Ocean Drilling Program (ODP) Leg 117, in the Indian Ocean (Figure 1). These sediments provide a natural archive of information on the Pleistocene history of upwelling, productivity and monsoon intensity along the Oman margin and Owen Ridge [e.g., *Shimmield et al.*, 1990; *Clemens and Prell*, 1991; *Weedon and Shimmield*, 1991]. *Bloemendal and deMenocal* [1989] previously identified the magnetic susceptibility variations of Hole 722B as an outstanding proxy record of paleoceanographic information. This susceptibility record correlates strongly with variations in the concentration and flux of eolian dust, displays Milankovitch periodicities (at frequencies of 100, 41, and 23-19 kyr), and contains a shift in its spectral character at 2.6 Ma, which possibly reflects the onset of major northern hemisphere glaciation [*Shackleton et al.* 1984]. Paradoxically, *Bloemendal et al.* [1993] reported that magnetic susceptibility maintained its strong correlation with the terrigenous component throughout the core, despite evidence of significant postdepositional loss of magnetic minerals through reductive diagenesis. Here we address this paradox, and examine further the paleoclimatic significance of the Site 722 susceptibility record by assessing the respective contributions to the bulk susceptibility signal of (1) ferrimagnetic detrital iron oxides, (2) ferrimagnetic iron oxides produced in situ by magnetotactic bacteria, (3) weakly magnetic (paramagnetic) detrital Fe silicate minerals, and (4) diamagnetic dilution by biogenic carbonate. While magnetic measurements provide a rapid, high-resolution means of sample differentiation, they cannot provide uniquely diagnostic information on mineralogy and mineral sources. Additional and complementary

Paper number 1998JB900085.
0148-0227/99/1998JB900085$09.00

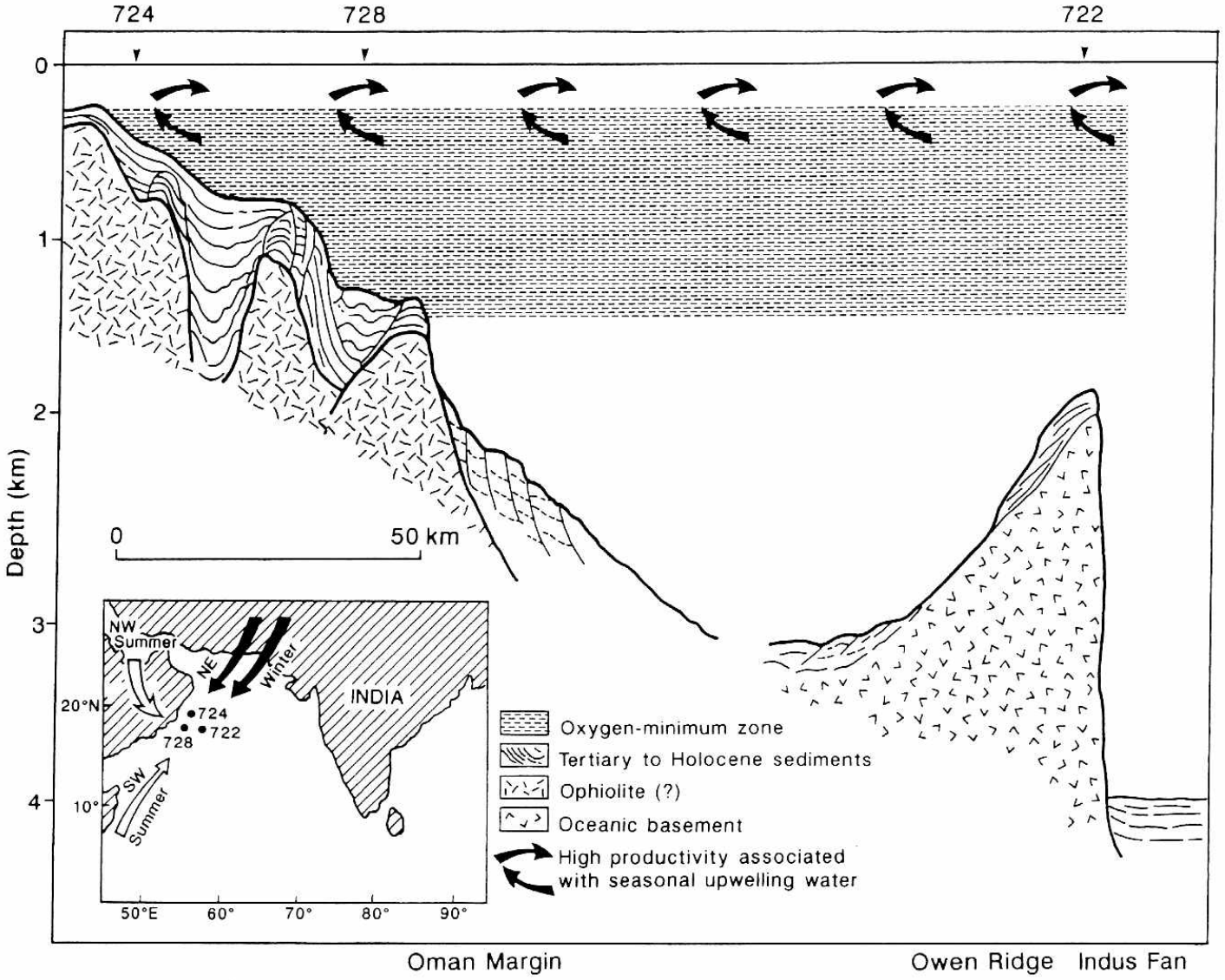

Figure 1. Location of ODP Hole 722B and directions of seasonal airflows [after *Prell et al.*, 1991], together with bathymetric cross-section of the Oman margin and Owen Ridge with respect to Leg 117 drill sites and the present oxygen minimum zone.

mineralogical data are required. These can be gained by subjecting a smaller number of representative samples to magnetic extraction procedures to concentrate the magnetic carriers. Chemistry, morphology and grain size can then be determined independently by X-ray diffraction (XRD), optical, scanning and transmission electron microscopy, and energy-dispersive X-ray analysis (EDXA). To ensure that magnetic extracts are representative of the original parent sample, before- and after-extraction magnetic measurements are performed, and the efficiency of the extraction is calculated. This combined magnetic and mineralogical approach enables precise identification of the key contributors to susceptibility at a site. Hence detailed definition of the magnetic/climatic connection can be obtained; the frequency of any climate-driven magnetic response, and its possible coherence with other climate indicators, can also then be assessed.

2. Study Site

To examine the relative impact of terrigenous magnetic mineral inputs and postdepositional effects on the susceptibility-climate link, we analyzed susceptibility data and Quaternary sediments from the Indian Ocean, from ODP Site 722 (Figure 1; *Prell et al.* [1989]). Within this region the Oman margin experiences seasonal upwelling that is induced by the southwest summer monsoon. As a result of the upwelling of cool, nutrient-rich water, biological productivity and organic decomposition rates are high and are responsible for the formation and maintenance of an intense oxygen minimum zone (OMZ) in the Arabian Sea. The OMZ presently extends from 200 m to ~1500 m in the water column [*Qasim*, 1982]. At a distance of 350 km from the coastal margin, the Owen Ridge runs roughly parallel to the Oman coast, rising 1500 m above the Oman Basin. At water depths of ~2000 m, it lies beneath the present position of the OMZ. The Owen Ridge is isolated from bottom-water-derived sediment, therefore its major detrital sediment source is eolian dust from Arabia and the Horn of Africa, with additional inputs from the Pakistan region [e.g. *Clemens and Prell*, 1991].

The whole-core magnetic susceptibility and $\delta^{18}O$ records for Hole 722B (water depth, 2028 m) are shown for the last 400 kyr in Figure 2. The susceptibility and oxygen isotope records are positively correlated, which is especially obvious over the last ~190 kyr when relatively large amplitude peaks in susceptibility coincide with heavier oxygen isotope values (indicative of glacial

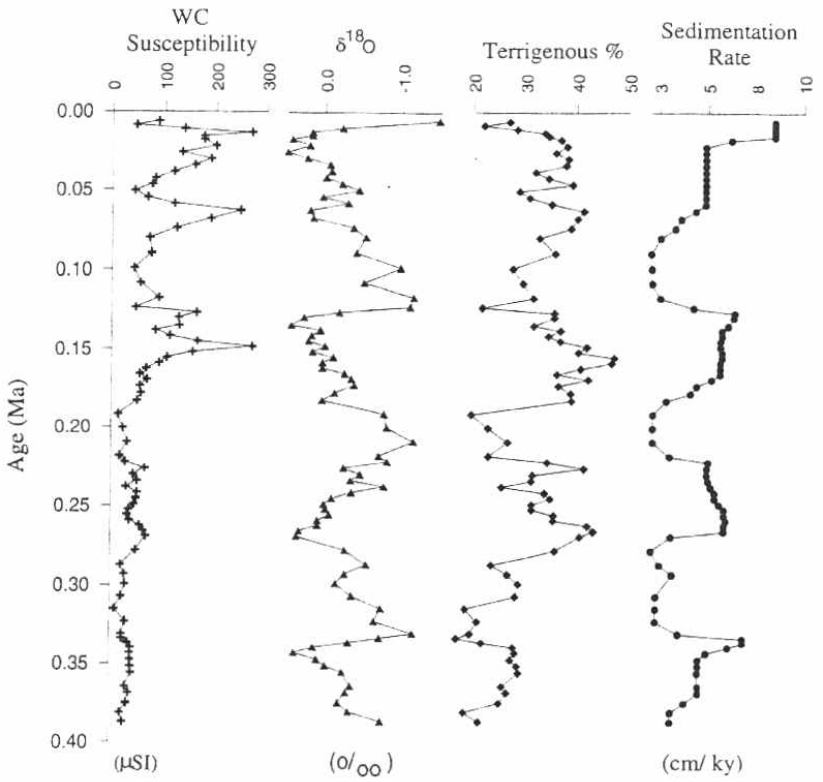

Figure 2. Whole-core susceptibility data, $\delta^{18}O$ values, terrigenous fraction (and, inversely, carbonate fraction) and sediment accumulation rate for Hole 722B for the last 400 kyr (from *Prell et al.* [1989], *Clemens and Prell* [1991], and *deMenocal et al.* [1991]).

stages). The whole-core susceptibility values also correlate positively with sediment accumulation rate and the terrigenous fraction, both of which are higher in glacial periods, but show negative correlation with calcium carbonate content (Figure 2, the carbonate content is the inverse of terrigenous percentage). The terrigenous component dominates the sediment mass accumulation rate and thus antithetically dilutes the carbonate signal. The carbonate flux exceeds the terrigenous flux, but the latter displays greater variations between glacial and interglacial periods (Figure 3).

2.1. Magnetic Susceptibility in Sediments

Magnetic susceptibility is the ratio of induced magnetization to the intensity of the magnetizing field. The low-field magnetic susceptibility of sediments (χ), which is normally measured at fields < 1 mT, can include contributions from a number of mineral components:

$$\chi_t = \chi_f + \chi_a + \chi_p + \chi_d, \quad (1)$$

where χ_t is the total susceptibility, χ_f is the susceptibility contributed by ferrimagnets such as magnetite, χ_a is the susceptibility from imperfect antiferromagnets and ferromagnets, such as hematite and goethite; χ_p is the susceptibility from paramagnets, such as Fe-bearing silicates; and χ_d is the negative susceptibility carried by diamagnetic minerals, such as calcium carbonate and quartz.

The susceptibility of ferrimagnetic minerals (up to ~57 x 10^{-6} m^3kg^{-1}) is orders of magnitude larger than that of imperfect antiferromagnetic (~0.5 x 10^{-6} m^3kg^{-1}), paramagnetic (~0.4 x 10^{-6} m^3kg^{-1}) or diamagnetic (-0.005 x10^{-6} m^3kg^{-1}) minerals (Maher,

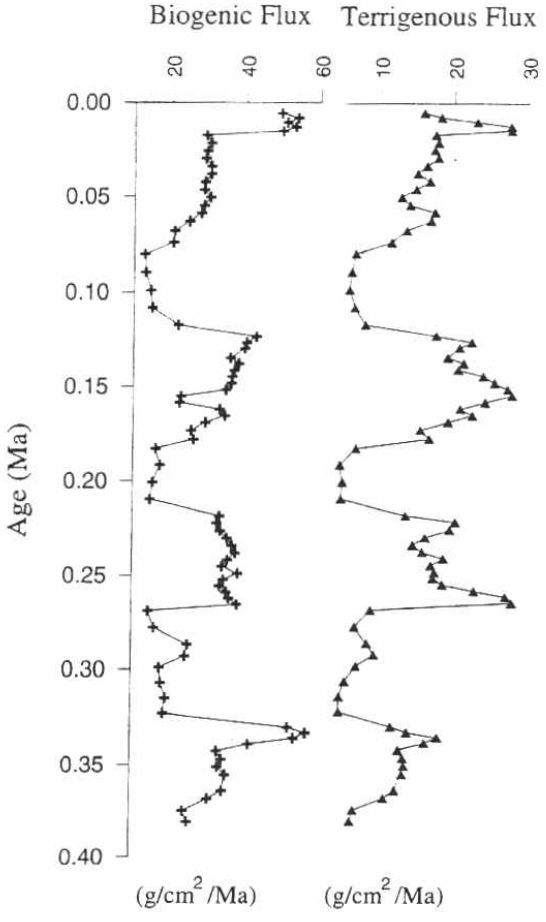

Figure 3. Fluxes of biogenic carbonate and terrigenous dust for Hole 722B for the last 400 kyr [from *Clemens and Prell*, 1991].

1998). Thus ferrimagnets often dominate the magnetic susceptibility of sediments, even when they occur in small amounts relative to other minerals. However, in ferrimagnet-deficient sediments, shifts in magnetic susceptibility can reflect changes in the other mineral components. In particular, the content of diamagnetic carbonate can vary greatly in deep sea sediments, as a consequence of changes in productivity and/or preservation, and can give rise to fluctuations in the total susceptibility due to "dilution effects" (even when the $\chi_f + \chi_a + \chi_p$ contribution may remain constant).

To understand in detail the origin of the magnetic susceptibility signal in sediments, it is necessary to decompose the magnetic susceptibility into its component contributions (equation (1)). It may then be possible to identify the environmental factors that have forced changes in susceptibility through the history of the sedimentary sequence.

2.2. Samples

The sediments from Hole 722B consist of foraminiferal ooze, with carbonate contents varying from 50 to 80%. Two sets of samples were examined: (1) a sample set taken at ~20-cm intervals from the top 14 m of Hole 722B, which was previously analyzed by nondestructive XRF measurements [*Shimmield et al.*, 1990], and (2) samples taken from Hole 722B at ~ 1-m intervals from 0.3 m below sea floor (mbsf) to 113 mbsf. Above 90 mbsf the sediments were cored by piston corer; below 90 mbsf a rotary extended core barrel (XCB) corer was used. We exclude the XCB-cored samples from further discussion here because analysis of their magnetic properties indicated that these lower sediments are contaminated by pipe rust from the XCB coring process.

2.3. Methods

The paramagnetic component of the susceptibility was estimated from low-temperature, low-field susceptibility measurements [*Richter and van der Pluijm*, 1994]. Paramagnetic minerals display temperature-dependent susceptibility, as described by the Curie-Weiss law:

$$\chi_p = C/(t - \theta), \qquad (2)$$

where C is the Curie constant, t is temperature (kelvins), and θ is the paramagnetic Curie temperature. Sediment samples were first cooled to liquid nitrogen temperature, then allowed to warm to room temperature; during the experiment, susceptibility and temperature were monitored continuously, using a Bartington Instruments MS2 susceptibility meter. To reduce the temperature gradient within the sample, an ethanol/glycerol mix was added as a wetting/conducting agent and thermal insulation was used. The paramagnetic component of the susceptibility was estimated by iterative modelling of the Curie-Weiss law to the measured low-temperature susceptibility of the samples (Figure 4). The numerical procedure is similar to that described by *Rochette and Fillion* [1988]. To avoid any possible susceptibility changes due to, for example, multidomain magnetic behavior, the portion of the susceptibility/temperature curve above the Verwey transition temperature was used for estimation of the paramagnetic component.

In order to evaluate the grain size, composition, and abundance of the remanence-bearing minerals in the Hole 722B sediments, measurements of anhysteretic remanent magnetization (ARM), isothermal remanent magnetization (IRM) and saturation isothermal remanent magnetization (SIRM) were made on sample sets a and b. ARMs were imparted in an alternating field of 80 mT with a bias field of 0.08 mT. The susceptibility of ARM (χ_{ARM}) was calculated by normalizing the ARM by the intensity of the applied bias field. IRMs were imparted in pulsed fields of 20, 50, 100, and 300 mT and in a steady dc field of 1000 mT. Where indicated, values are expressed on a carbonate-free basis (e.g. χ_{cf}, $SIRM_{cf}$), i.e., they are normalized by the mass of the noncarbonate content of the sample. Carbonate contents were calculated from XRF analyses, using the procedure detailed by *Shimmield and Mowbray* [1991].

To identify the mineralogy, magnetic grain size, and relative contributions of the magnetic minerals in the Hole 722B sediments, quantitative magnetic extraction procedures were applied to 21 representative samples, using the magnetized probe method [*von Dobeneck*, 1985; *Hounslow and Maher*, 1999]. Prior to magnetic extraction, the samples were decalcified using buffered acetic acid and were then particle sized into <38-μm and >38-μm fractions. The decalcification procedure was previously reported to cause dissolution of ultrafine magnetic grains [*Sun and Jackson*, 1994]; a subsequent study [*Hounslow and Maher*, 1996] indicates that this is not the case. The extraction procedures produce up to four magnetic separates: (1) grain sizes larger than 38 μm, (2) grain sizes from 38 μm to ~1 μm, (3) grain sizes smaller than ~1 μm, and (4) the paramagnetic fraction (with

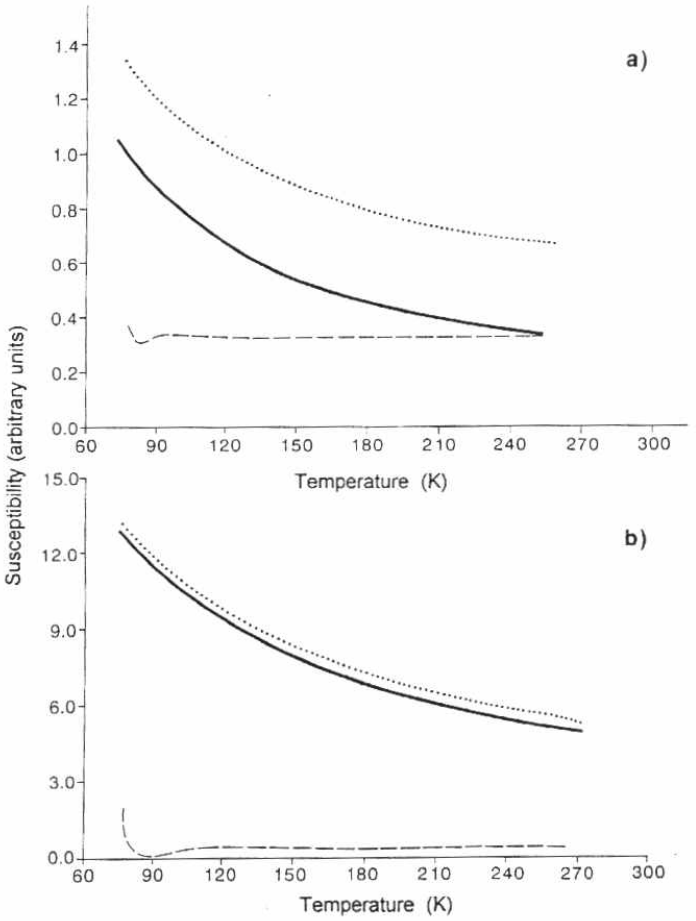

Figure 4. Low-temperature susceptibility measurements (with instrument drift removed) for Hole 722B samples: (a) sample depth of 2.25 mbsf; (b) sample depth of 6.81 mbsf. The dotted line shows measured susceptibility data, the solid line is a fitted paramagnetic curve over the range indicated, and the dashed line is the residual (measured susceptibility data minus the paramagnetic curve).

Table 1. Data for Magnetic (E_{MP}) Extracts (<38 μm, after carbonate dissolution)

Sample Depth, mbsf	Magnetite lattice constant *a*, Å	E_{MP}/ Wt_{fine}, wt %	IRM/ IRM_t, %	Extraction Efficiency, %			Minor minerals
				χ	ARM	IRM	
0.35[a]	8.381	1.02	99.8	63	70	82	prx, hor, chl, spi, mic
1.25[a]	8.379	0.890	99.7	66	59	79	prx, hor, to, zi, rut,mic
2.25[a]	8.395	0.556	99.9	41	71	76	hor, chl, mic, zi, rut
3.27[a]	8.378	0.532	99.9	55	87	77	rut, hor, chl, mic, spi
4.24[a]	8.390	0.452	98.8	30	57	81	rut, hor, chl, mic, zi, spi
5.23[a]	8.393	0.510	99.9	48	90	83	rut, hor, chl, mic, spi
5.81[a]	8.374	0.284	99.4	49	45	82	rut, hor, zi, chl, mic, apa, dol, spi, mic
7.8[a]	8.392	0.192	99.9	11	15	73	rut, mic, hor, chl, apa, spi
9.73[a]	8.410	0.135	99.9	32	49	71	rut, horn, mic, spi, chl, apa
11.77[a]	8.384	0.081	99.9	9	55	70	rut, hor, spi, dol, prx, apa, mic
13.80[a]	[b]	0.186	99.8	28	65	75	rut, mic, spi, hor, mic, prx, apa, kya, zi
15.57[a]	[b]	0.166	99.4	25	68	79	rut, hor, prx, mic, chl, zi, spi, apa
17.42[a]	8.391	0.202	99.5	0	49	74	rut, mic, spi, prx, zi, hor
19.42[a]	8.374	0.132	99.0	13	9	49	mic, chl, hor, rut
21.42[a]	[b]	0.114	99.1	3	36	70	mic, chl, hor, rut
26.8-29.0	[b]	0.245	65.3	13	18	60	mic, chl, hor, rut
38.6	8.383	0.071	97.6	17	33	51	mic, chl, hor, rut
40.6	8.369	0.111	96.3	10	7	54	mic, chl, hor, rut
60-62	[b]	0.503	95.1	0	38	55	mic, chl, hor, rut
1.87-6.97 (G)	8.379	0.100	91.9	62	59	86	mic, chl, hor, rut
2.37-6.97 (I)	8.377	0.193	88.3	15	83	78	mic, chl, hor, rut

IRM/IRM_t is the ratio of the SIRM of the <38-μm fraction to that of the bulk sample. E_{MP}/wt_{fine} is the weight percent of the MP extract compared to the sample weight used in the MP extraction. Minor minerals are rut, TiO_2; hor, hornblende; prx, pyroxene; zi, zircon; mic, micas; chl, chlorite; spi, red/brown spinel; apa, apatite; kya, kyanite; to, tourmaline; and dol, dolomite. G indicates a composite sample, comprising an amalgam of samples from glacial periods within the interval shown, and I indicates a composite sample from interglacial periods.

[a] For these samples the <63-μm fraction was used in MP separation.

[b] Peak was too broad or low in intensity for reliable lattice spacing determination.

no grain size dependence). The amount of magnetic material extracted at each stage was quantified by before- and after-extraction magnetic measurements (susceptibility, ARM, and IRM). The extraction efficiencies are listed in Table 1.

The major and minor mineral phases in the magnetic separates were identified by X-ray diffraction (XRD), using a Philips PW1710 X-ray diffractometer with monochromatic Cu radiation, automatic divergence slit and scan speed of 0.005° 2θ s^{-1}. Semiquantitative estimates of the major mineral abundances were obtained by calibration of the diffractometer, using binary mixtures of mineral standards and quartz. Mineral peak areas were determined with a peak-fitting algorithm (supplied by Philips Ltd), and were used to estimate mineral abundance, following the methods detailed by *Hooten and Giorgetta* [1977] and *Hounslow and Maher* [1999]. The position of the magnetite [511] peak was used to estimate the spinel unit cell dimension, using the quartz [112] peak as an internal reference. Clay minerals in the paramagnetic extracts were identified by a sequence of XRD measurements on a subsample that was treated with glycol vapor for 12 hours, then heated at 300°C and at 500°C [*Brindley*, 1980].

Optical microscopy provided information on the grain size, morphology, composition and mineral interrelationships for the magnetically extracted grains larger than ~1 μm. It also enabled identification of the presence and significance of ferrimagnetic inclusions within various silicate minerals. Scanning electron microscopy (SEM, Hitachi S450) was used to examine the morphology of the magnetic minerals larger than ~1 μm in size, and also for identifying the elemental composition of these grains, using EDXA (Link Systems Ltd). For examination of the ultrafine (<~1 μm) magnetic separates, we used TEM (JEOL 100CX) and EDXA.

3. Results

3.1. Paramagnetic/Diamagnetic Contributions to the Susceptibility

First, the contribution of varying amounts of diamagnetic carbonate to the volume magnetic susceptibility record is evident from Figure 5. By expressing the single-sample susceptibility data on a carbonate-free basis, the amplitude of variation in susceptibility is significantly diminished. Thus the original whole-core volume susceptibility record can be dominantly perceived as a measure of carbonate variations (or, inversely, as terrigenous percent variations).

Typical results from low-temperature measurements of susceptibility on single sediment samples are shown in Figures 4a and 4b, together with the fitted paramagnetic curves, the residuals, and the estimated paramagnetic/ferrimagnetic ratios. For the sample from 2.25 mbsf, the paramagnetic contribution to susceptibility amounts to 48% (Figure 4a). For the sample from

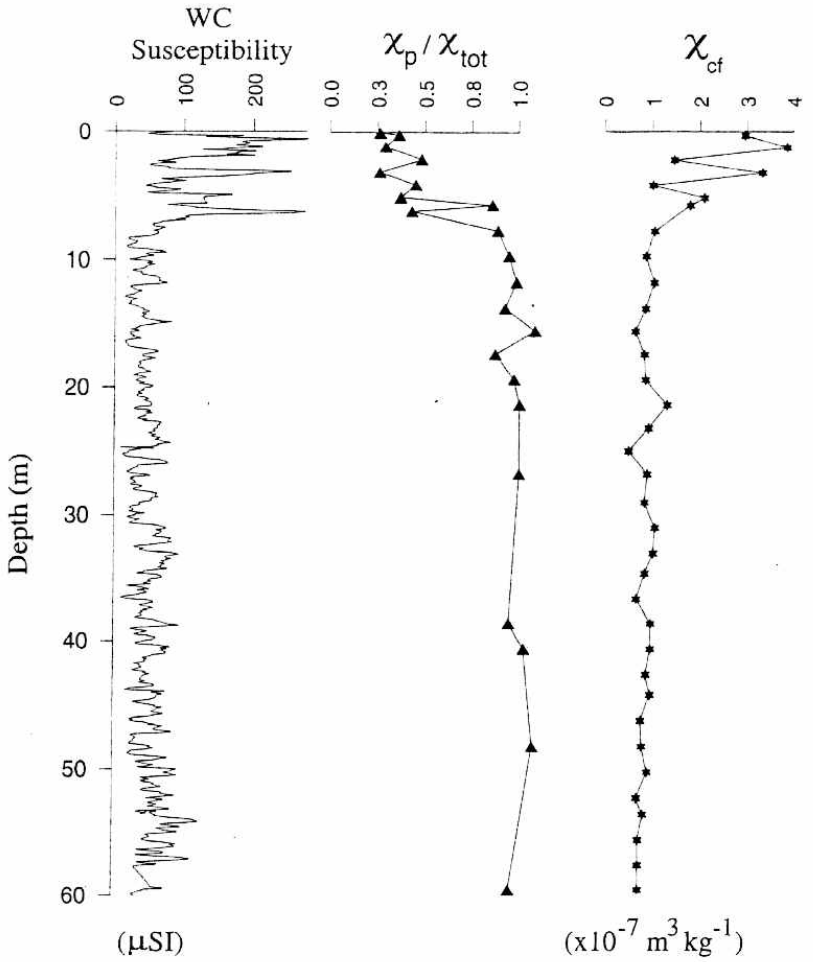

Figure 5. Whole-core magnetic susceptibility, the calculated paramagnetic proportion of the susceptibility signal and the carbonate-free magnetic susceptibility, from single samples, for the last 400 kyr in Hole 722B.

6.81 mbsf, the paramagnetic contribution is 94% (Figure 4b). After removal of the paramagnetic component, the low-temperature susceptibility data do not display the Verwey transition. Within the upper ~7 m of Hole 722B, peaks in carbonate-free susceptibility and SIRM (Figures 5 and 6) are associated with lower paramagnetic contributions (~30%) and troughs are associated with higher paramagnetic proportions (~45%). Below ~7 mbsf the paramagnetic contribution to susceptibility varies between 85 and 100%. Thus in Hole 722B the only part of the susceptibility record that is significantly influenced by ferrimagnetic minerals occurs within the top ~7 m of the core (Figure 5). This finding contradicts the assumptions made by *Bloemendal et al.* [1993] of a ferrimagnetic source for the Hole 722B susceptibility record.

3.2. Ferrimagnetic and High-Coercivity Components

The IRM data indicate that the magnetic remanence properties of the Hole 722B sediments are dominated by a magnetite-like phase, with a relatively small contribution from a high-coercivity source (hematite or goethite). Most magnetization is acquired in fields of less than 100 mT. On the basis of the magnetic remanence parameters (Figures 6 - 8), the sediments from 0 - 90 mbsf can be divided into five zones, as follows.

3.2.1. Zone 1 (0 - 1.7 mbsf). The highest values of susceptibility, χ_{ARM}, and SIRM occur within the top 1.7 m of Hole 722B. This is particularly the case for χ_{ARM}, which increases by an order of magnitude over the interval from 1.7 - 1.2 mbsf (Figure 6). The χ_{ARM}/SIRM ratio also increases markedly across this interval which indicates, for these magnetite-dominated samples, a decrease in magnetic grain size [e.g., *Özdemir and Banerjee*, 1982; *Maher*, 1988]. IRM acquisition measurements indicate strong concomitant changes in the percentage of the remanence acquired (Figure 7) both at low fields i.e., between 0 and 20 mT ($\%IRM_{0-20\ mT}$), and between 50 and 100 mT ($\%IRM_{50-100\ mT}$).

3.2.2. Zone 2 (1.7 - ~7 mbsf). Over this interval, both χ_{ARM} and χ_{ARM}/SIRM are relatively stable (Figure 6). In contrast, χ_{cf}, $SIRM_{cf}$ and the remanence acquired at high (>300 mT) fields (HIRM) vary in correspondence with glacial to interglacial climate oscillations (Figure 6). Several of the remanence fractions also display strong glacial/interglacial variations, especially $\%IRM_{100-300\ mT}$ (Figure 7). During glacial stages, χ_{cf} and $SIRM_{cf}$ are high, and the amount of paramagnetic material is reduced. Conversely, $\%IRM_{100-300\ mT}$ increases during interglacial stages (Figure 7). This cyclicity is most marked for parameters that reflect magnetic abundance, with enhanced ferrimagnetic contributions during glacial periods. The magnetic contrast across the zone1/zone 2 boundary indicates that the grain size of the ferrimagnetic particles is coarser in zone 2 than in zone 1. Declining HIRM but higher $\%IRM_{0.3-1\ T}$ values indicate lower absolute amounts of high coercivity phases such as hematite and/or goethite, but increased concentrations of these phases relative to the ferrimagnetic component in zone 2 with respect to zone 1.

3.2.3. Zone 3 (~7 - 10.5 mbsf). From ~7 to 10.5 mbsf, susceptibility, χ_{ARM}/SIRM and SIRM all have low values and display changes that do not correspond to glacial/inter-glacial

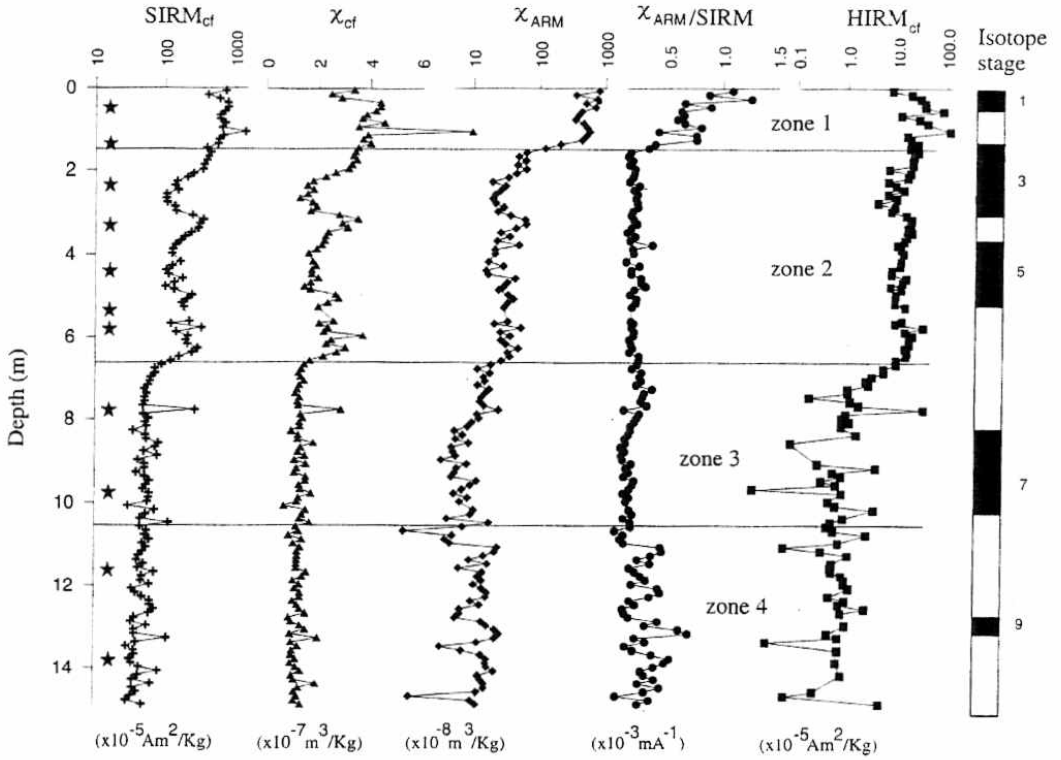

Figure 6. SIRM, susceptibility, χ_{ARM}, χ_{ARM}/SIRM and HIRM data for the top 15 m of Hole 722B, together with assigned magnetic zones (see text for details) and oxygen isotope stages. All the magnetic data are expressed on a mass-specific, carbonate-free basis. The stars on the depth axis correspond to the position of samples that were subjected to magnetic extraction.

cyclicity (Figure 6). This is shown by SIRM, for example, which abruptly changes in the middle of isotope stage 6 and by χ_{ARM}/SIRM which changes in the middle of isotope stage 8 (Figure 6). The zone 2/zone 3 boundary (at ~6.7 mbsf) is defined by changes in each of the remanence fractions (Figure 7). The high-coercivity component also displays a marked response at this level; it declines both in terms of its abundance (HIRM) and its relative contribution to the SIRM in zone 3 compared to zone 2 (Figure 7). However, this boundary is not as sharp for either χ_{ARM} or χ_{ARM}/SIRM, which decay slowly over the interval from 7 – 8 mbsf. Below 7 mbsf, detection of the 0.3 - 1 T contribution to the IRM is close to the noise limit of the magnetometer.

3.2.4. Zone 4 (10.5 - ~22 mbsf). At the zone 3/zone 4 boundary, ferrimagnetic grain size decreases (as indicated by

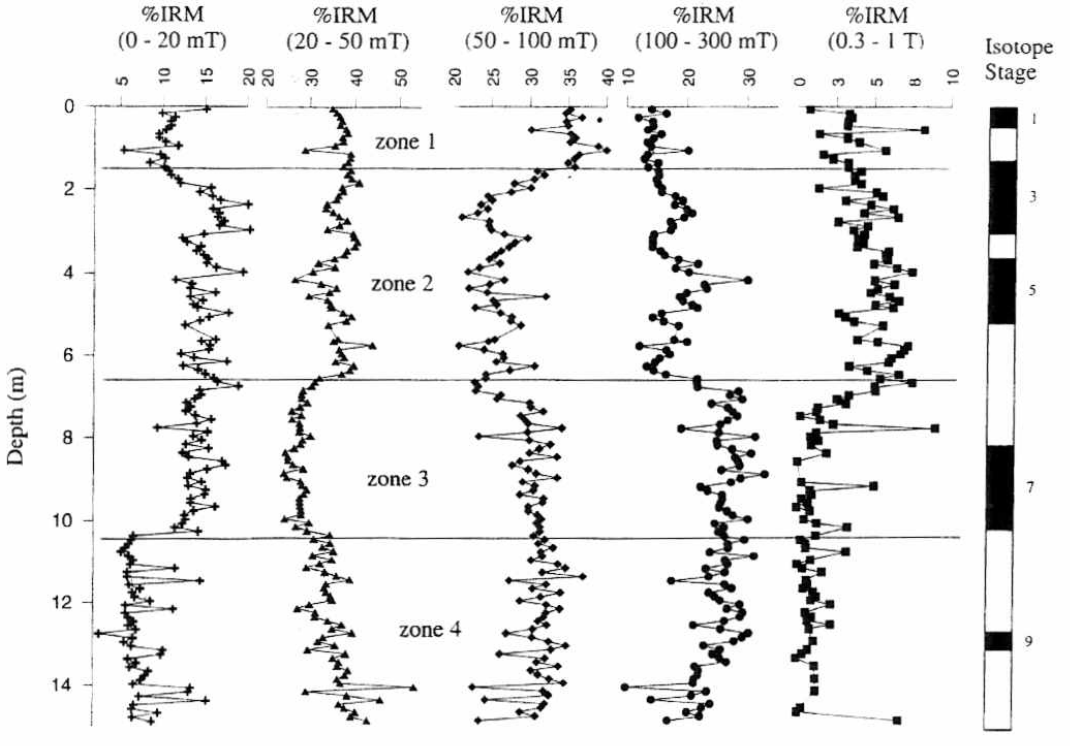

Figure 7. Percent IRM acquisition in applied fields of 0 - 20, 20 - 50, 50 - 100, 100 - 300 mT and 0.3 - 1 T in the upper 15 m of Hole 722B, together with assigned magnetic zones.

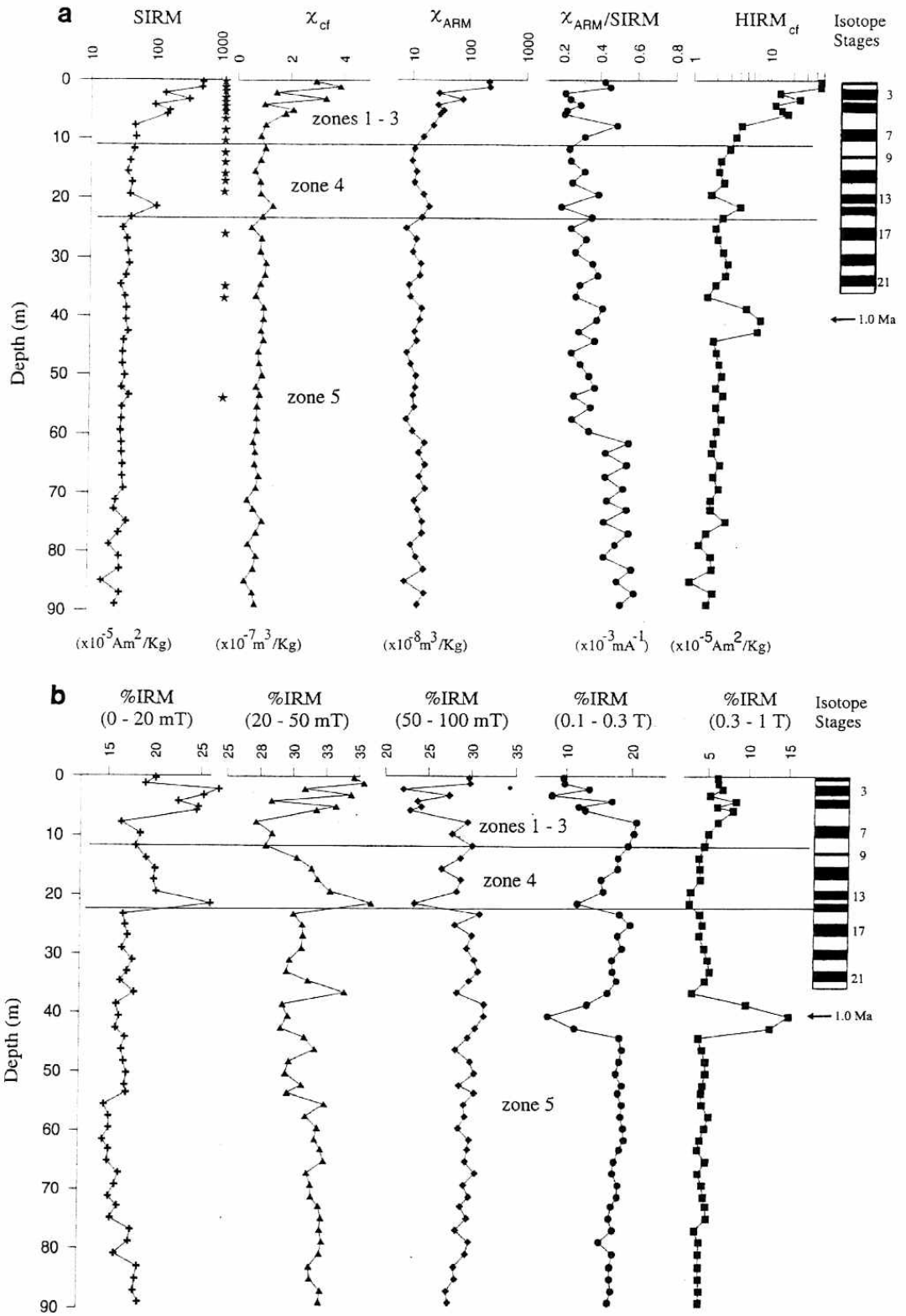

Figure 8. (a) SIRM, susceptibility, χARM, χ_{ARM}/SIRM, and HIRM data for the upper 90 m of Hole 722B. The stars on the depth axis correspond to the position of the magnetic extracts. All the magnetic data are expressed on a mass-specific carbonate-free basis. (b) Percent IRM acquisition data for the same interval. Assigned magnetic zones are also shown.

lower values of %IRM$_{0-20\ mT}$ (Figures 7 and 8b). This change in zone 4 partly reverses the changes observed at other boundaries in the upper part of the hole. Zone 4 is marked by a progressive downhole increase in %IRM$_{0-20\ mT}$ and %IRM$_{20-50\ mT}$, and a decrease in %IRM$_{0.3-1\ T}$ (Figure 8b).

3.2.5. Zone 5 (~22 - 90 mbsf). Within zone 5 (Figure 8a and b), the remanence parameters and susceptibility are generally stable, with the exception of HIRM, %IRM$_{0.3-1\ T}$ and %IRM$_{0.1-0.3\ T}$, which respond to changes in the high-coercivity component. These show a marked shift between ~38 and 45 mbsf, which is indicative of an increase in the amount of high-coercivity material, with HIRM values almost as high as those in the top 7 m of the hole. The mineralogical origins of the zone 4/zone 5 transition are not readily apparent from the magnetic data alone. Below 56 mbsf, χ_{ARM}/SIRM, χ_{ARM} and %IRM$_{20-50\ mT}$ also gradually increase.

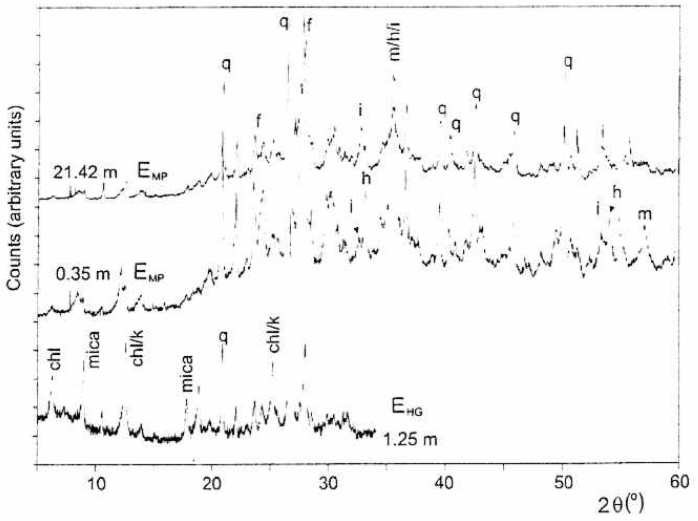

Figure 9. X-ray diffraction data for E_{MP} extracts from 0.35 mbsf and 21.42 mbsf and for the clay-dominated, E_{HG} (high-gradient) extract from 1.25 mbsf. Minerals are q, quartz; f, feldspar; i, ilmenite; h, hematite; m, magnetite; chl, chlorite; and k, kaolinite.

3.3. Magnetic Mineralogy From Magnetic Extracts

For these fine-grained sediments, the ferrimagnetic properties are dominated by the <38-μm fraction, as is shown by the ratio of the IRM of this fraction to that of the bulk sample (IRM/IRM_t, Table 1). This ratio varies between 65 and 99.9% but has a mean value of 96.6%. Furthermore, for each of the samples subjected to magnetic extraction, the bulk of the magnetic material was recovered from the ~1- to 38-μm extract, which indicates that most of the ferrimagnetic material is present in this fraction.

3.4. Extraction Efficiencies

For the upper ~7 m of sediment, the extraction efficiency ranges from 45 to 90% for ARM, from 76 to 83% for SIRM, and from 30 to 66% for susceptibility (Table 1). Below ~7 mbsf, extraction efficiencies generally decline downhole, reflecting marked changes in the magnetic mineralogy with depth (as discussed below). Particularly notable is the steep decline in susceptibility extraction efficiencies, which fall to very low values (0 - 32%). This is due to the domination of susceptibility by paramagnetic minerals in the interval below ~7 mbsf. Such minerals are relatively poorly extracted by the magnetized probe procedure [*Hounslow and Maher*, 1996]. Below ~7 mbsf, 49 - 79% of the SIRM and 7 - 68% of the ARM are extracted.

3.5. Mineralogy of the Magnetic Extracts

By mass, the extracts obtained by the magnetized probe process (E_{MP}) are dominated by quartz and feldspar (predominantly sodic plagioclase with some K feldspar). Other major components of the extracts are magnetite, hematite, and ilmenite (Figure 9), and pyrite and rutile. Pyroxenes, amphiboles, micas, brown and red spinels, zircon, chlorite, dolomite, apatite, and kyanite (Table 1) occur as minor components (<5%). The reason for the abundance of quartz and feldspar in the extracts is the common occurrence of ferrimagnetic inclusions within the silicates (Figure 10) [*Hounslow and Maher*, 1996]. Other paramagnetic phases (ilmenite, pyroxenes, amphiboles, micas) are also present in the extracts owing to either ferrimagnetic inclusions or a relatively high paramagnetic susceptibility. Pyrite is present in the extracts because the pyrite grains either enclose, or are attached to, ferrimagnetic particles.

EDXA analyses of the extracts indicate the presence of both low-Ti magnetites and magnetites with no substitution by Ti. The spinel lattice constant of the magnetite phase in the extracts varies between 8.37 to 8.41 Å (Table 1). Averaging the values above and below 7 mbsf in the core gives 8.383 and 8.386 Å, respectively, which indicates that there is no systematic difference through the core in the composition or oxidation state of the magnetite. These lattice constants suggest that on average, the magnetites are partially oxidized, with an oxidation parameter of $z = 0.4 - 0.6$ [*Keefer and Shive*, 1981]. However, XRD peaks for the spinels are sometimes broadened, suggesting that there is some intergrain variation in either composition and/or oxidation state.

3.6. Abundances of Magnetite and Hematite

To determine the abundance of the remanence-carrying phases in the original sediment, the following procedure was used. Assuming that the IRM acquired between 0 and 100 mT is proportional to the amount of magnetite present, and that acquired between 0.3 and 1 T is proportional to the amount of hematite, the amounts of each mineral can be determined from the extraction efficiency of these remanence fractions, and from the original sediment IRM values, and their relative proportions in the extracts, as measured by XRD [*Hounslow and Maher*, 1999]. These calculations indicate that there is a gradual, but marked downcore loss of the magnetite and hematite within the first 7 m of Hole 722B (Figure 11). There is greater loss of magnetite, compared to hematite, over the interval 0-2 mbsf. These data are in accord with χ_{ARM} and SIRM data which decline more rapidly than the HIRM in this interval (Figure 6). For the interval ~2 - 7 mbsf, the calculated magnetite and hematite abundances fluctuate in parallel with glacial/interglacial cyclicity, with higher contents

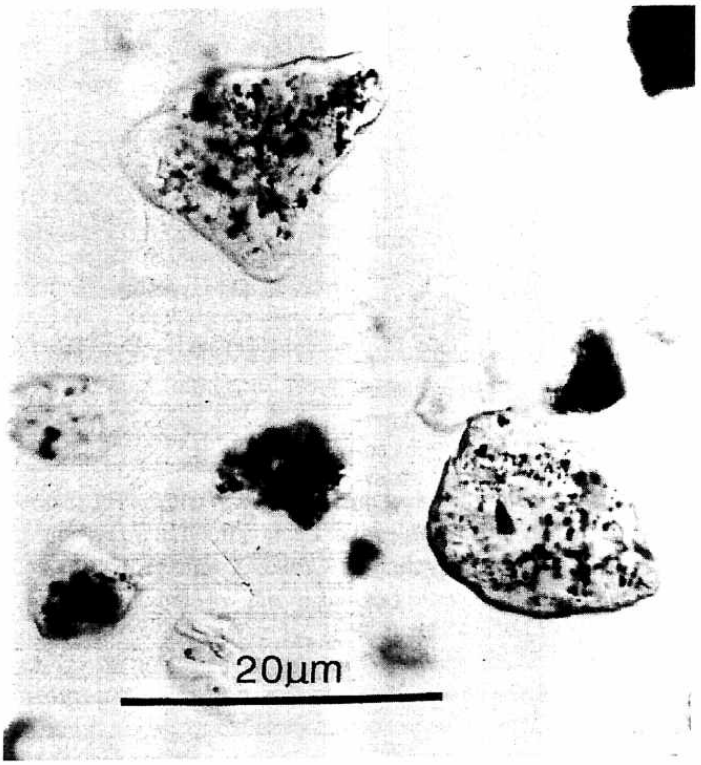

Figure 10. Optical micrograph of magnetic inclusions within quartz host grains.

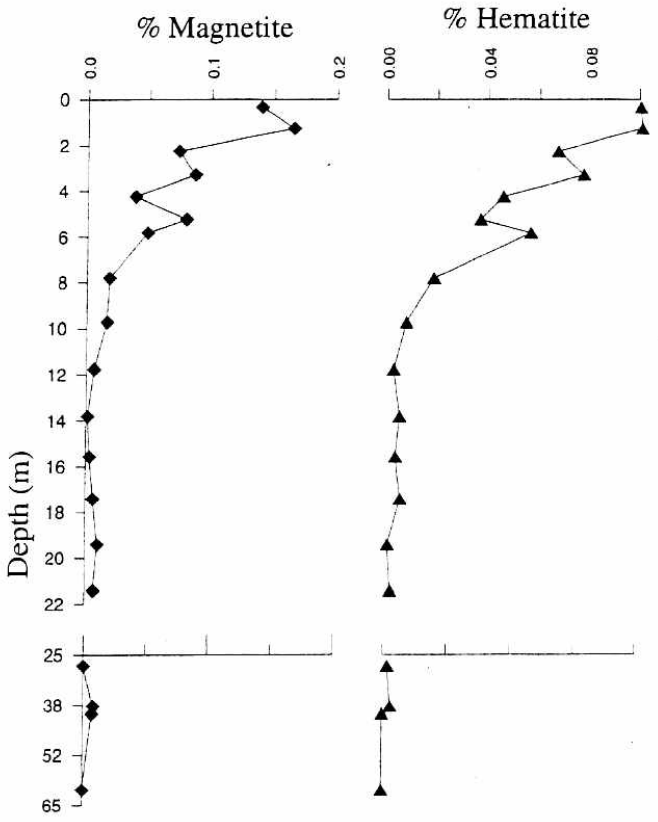

Figure 11. Percentages of magnetite and hematite in the original sediment, as estimated from semiquantitative XRD on magnetic extracts (see text for details).

of each during glacial periods. From reflected light microscopy, the hematite is common as coatings (with characteristic red internal reflections) on magnetite and ilmenite particles. The presence of hematite in this form is readily evident only from optical microscopy; such coatings are not chemically or morphologically apparent in SEM analyses of the extracts.

The marked decline in the magnetite and hematite content with depth probably results from destruction by diagenesis associated with sulfate reduction. This is evident by the appearance of pyrite framboids in the sediment at 0.35 mbsf (Figure 12). Analysis of the pore water chemistry of Hole 722 sediments [*Pedersen and Shimmield,* 1991] indicates progressive net consumption of sulfate from the near-surface, reaching minimal values (1 mmol/L) at ~100 mbsf. The pore water and magnetic data thus indicate that the Fe reduction zone occurs within the top 1 m of sediment at this upwelling site. Loss of the discrete detrital magnetic grains seems to occur primarily by a process of iron dissolution rather than by direct, in situ replacement by sulfides [*Canfield and Berner*, 1987]. Optical microscopy of the extracts shows that the pyrite occurs as small (~2 - 10 μm) framboids or as scattered microcrystals. We found no evidence for magnetic iron sulfides, such as greigite.

3.7. Magnetic Mineralogy of Zones 1 - 5

Within the magnetic extracts from the top ~1.7 m, we found a bimodal population of magnetic grains (Figure 13a). By far the dominant component comprises fine grains (~2 - 3 μm) of lithogenic titanomagnetite (Figure 13b). The second component consists of distinctive ultrafine Fe-oxide crystals, of controlled grain size (~0.05 μm) and morphology (Figure 13a). These are diagnostically of biogenic origin, formed intracellularly by magnetotactic bacteria. These magnetosomes are present only in minor quantities (<1% of the <1-μm magnetic separate), and do not make a major contribution to the bulk magnetic properties of the sediment. However, because of their submicron size and the interactions between the magnetosome grains, they contribute preferentially to ARM [e.g., *Özdemir and Banerjee*, 1982; *Maher*, 1988; *Dunlop and Argyle*, 1997]. TEM observations indicate that below ~1.7 mbsf in Hole 722B, the numbers of both bacterial magnetosomes and lithogenic, fine-grained titanomagnetite crystals decrease dramatically, leaving a residue of coarser-grained lithogenic titanomagnetites. This change is seen in the

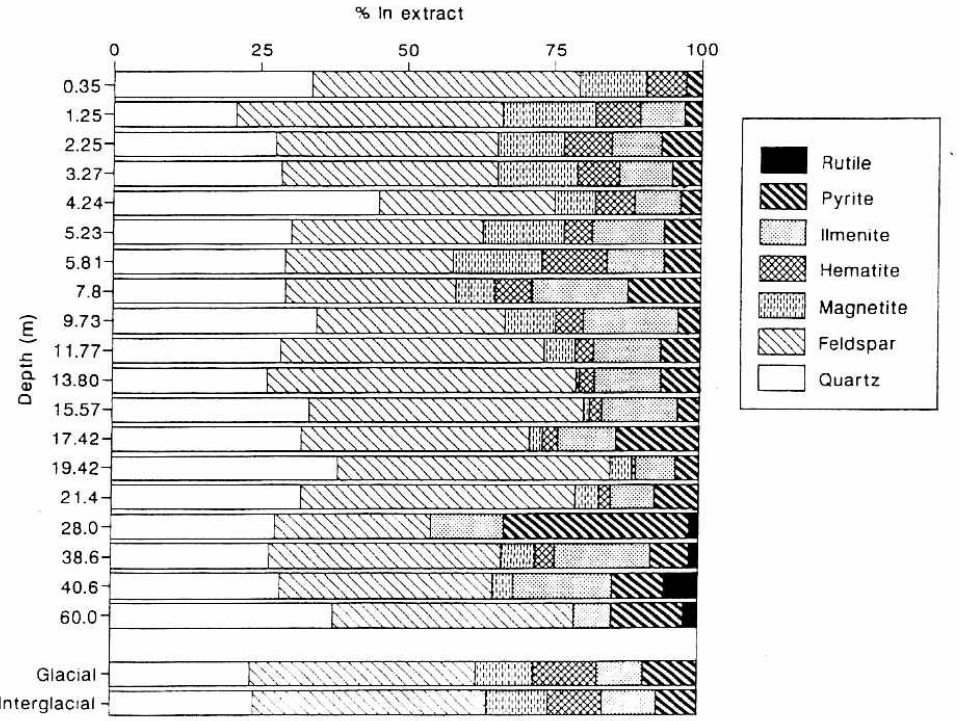

Figure 12. Relative amounts of major minerals in the magnetic extracts, determined by semiquantitative XRD analysis. The "glacial" and "interglacial" samples are composite samples from the depth range 1.87 - 6.97 mbsf.

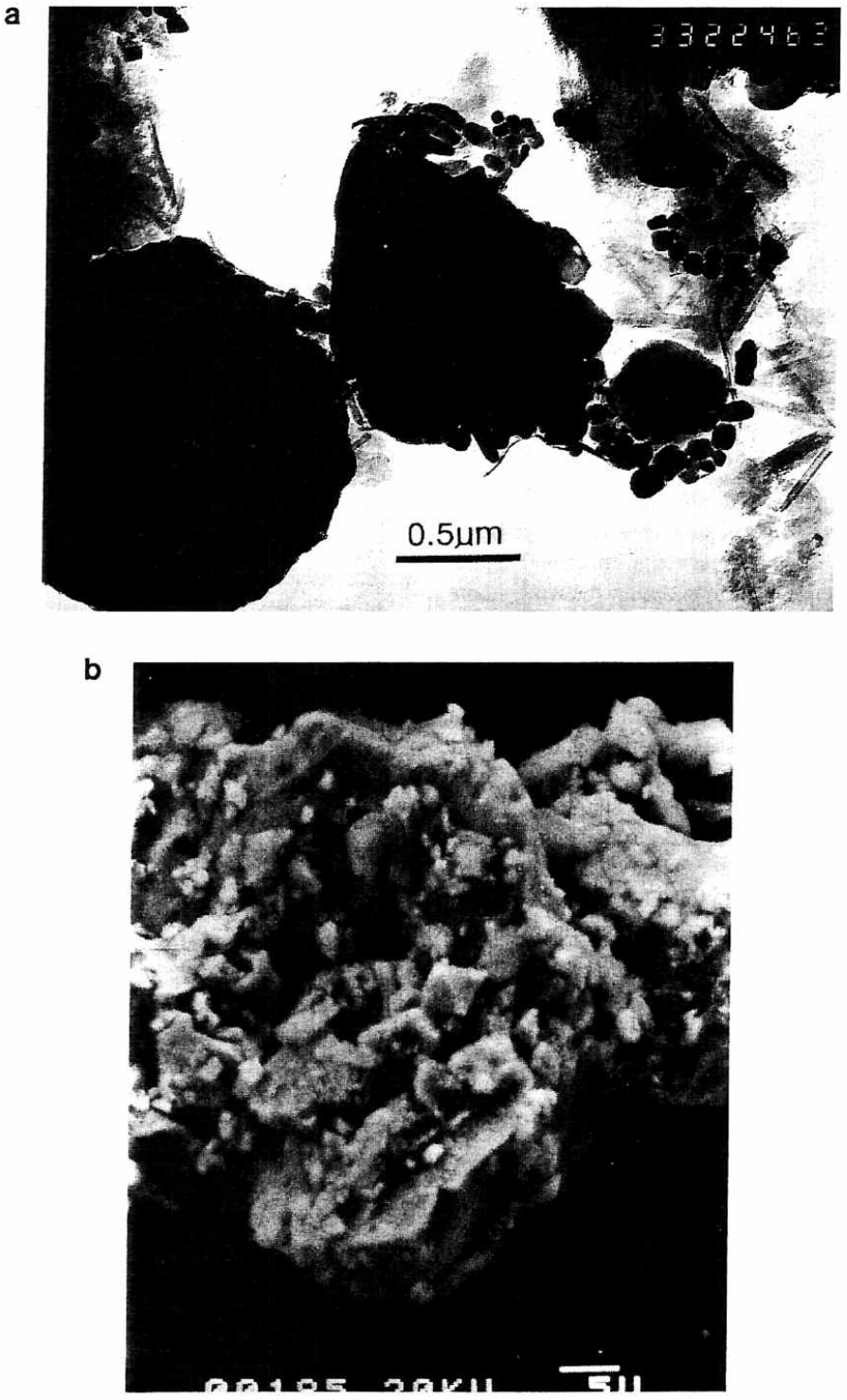

Figure 13. (a) Transmission electron micrograph of bimodal population of fine and ultrafine magnetic grains from 1.25 mbsf, Hole 722. (b) Scanning electron micrograph of fine-grained lithogenic titanomagnetites from 1 mbsf, Hole 722B.

magnetic parameters, particularly by the marked decline in χ_{ARM}/SIRM, and also in the magnetite abundance estimates (Figure 11). Thus the mineralogical data demonstrate that the zone 1/zone 2 magnetic transition is due to the loss of discrete fine and ultrafine magnetic grains of both lithogenic and biogenic origin.

In contrast, the mineralogy of the magnetic particle population in zone 2 appears more stable, both during glacial and interglacial stages, with Fe-Ti oxide particles mantled with an oxidative coating of hematite. Within this interval, changes in the magnetic properties (χ_{cf}, $SIRM_{cf}$) indicate fluctuations in the amount of magnetic material (higher concentrations during the glacial period). The one major mineralogical difference is the higher paramagnetic mineral content in the interglacial sediment.

Across the zone 2/zone 3 boundary (at ~7 mbsf), the most dramatic change in the magnetic properties is a significant downcore decline in the χ_{cf}, HIRM and $\%IRM_{0.3-1T}$ (Figures 6 and 7). At this boundary the susceptibility signal changes from a mixture of paramagnetic and ferrimagnetic contributions (above ~7 mbsf) to one dominated by paramagnetic minerals (Figure 5). In the extracts from zones 2 and 3, the most notable mineralogical changes are the loss in zone 3 of the oxic coatings on many grains and an increase in the content of TiO_2 particles. These indicate dissolution of the hematite grains and coatings and the removal of

Fe from Fe-Ti oxides, to produce relict TiO_2 [cf. *Morad and Aldahan*, 1986].

In zones 4 and zone 5, three mineralogical factors are increasingly important: (1) the dominance of ilmenite in the magnetic extracts over XRD-detectable magnetite; (2) the disappearance of discrete detrital magnetic Fe-Ti oxides; and (3) the increasing importance of magnetic inclusions in detrital silicates. The fining of magnetic particles at the zone 3/4 transition, as indicated by an increase in χ_{ARM}/SIRM and a fall in the low coercivity IRM fraction (%IRM $_{0-20\ mT}$), may reflect two different factors. First, selective removal of iron from the coarse titanomagnetite grains may result in a reduction in grain size and to their eventual loss by dissolution. Second, as the discrete magnetic grains are dissolved, the relatively finer-grained inclusions may make a progressively greater contribution to the total magnetization.

It should be noted that analysis of unpolished magnetic extracts by SEM alone (i.e., without XRD) could lead to the mistaken identification of ilmenite as titanomagnetite, because neither morphology nor EDXA enable differentiation between these minerals. Previous authors [*Bloemendal et al.*, 1993] have, on this basis, misattributed a downhole increase in Ti content in Hole 722B to an increased concentration of titanomagnetite. Ilmenite has been reported to display greater stability than magnetite or hematite under reducing diagenetic conditions [e.g., *Dimanche and Bartholome*, 1976; *Canfield et al.*, 1992], as is also evidenced by mineralogical data in thus study. The declining downhole abundances of magnetite and hematite are also recognized with XRD. Concomitant increases in the relative importance of transparent silicates, pyrite, and relict TiO_2 are evident from optical microscopy and from the declining magnetic extraction efficiencies (Table 1) [*Hounslow and Maher*, 1996].

It is difficult to define the origins of the magnetic changes below ~35 mbsf in the Hole 722 sediments. At ~55 mbsf the shift toward higher χ_{ARM}/SIRM ratios may again relate to a progressively increasing magnetic contribution from fine grained inclusions. At ~40 mbsf, the notable spikes in HIRM and %IRM $_{0.3-1\ T}$ may indicate changes in the abundance and/or the grain size of the high coercivity minerals, whether as discrete particles or as inclusions.

3.8. Source of the Paramagnetic Susceptibility Signal

The susceptibility extraction efficiencies (Table 1) indicate that ~5 to 30% of the susceptibility is carried by the minerals recovered in the E_{MP} extracts and that more than 95% of the susceptibility signal (below ~7 mbsf) is carried by paramagnetic minerals. Paramagnetic minerals identified in the E_{MP} extracts include Fe-bearing silicates and oxides, ilmenite, chlorite, hornblende, and pyroxene. However, 70 - 95% of the susceptibility signal is carried by minerals concentrated in the 'non-magnetic' residues from the magnetic extraction.

To extract and identify the paramagnetic minerals from the residues, a high-gradient, high magnetic field (1 T) extraction procedure was used [*Righi and Jadualt*, 1988; *Hounslow and Maher*, 1996]. This procedure enabled extraction of large amounts (10 - 28% by weight) of weakly magnetic material from the samples, typically resulting in a 30% reduction in the susceptibility of the residues. These extracts are dominated by chlorites, micas, and kaolinites, with subsidiary smectites, together with quartz, plagioclase, and hornblende (Figure 9). These data indicate that the paramagnetic susceptibility of the sediments is carried by a variety of Fe-bearing silicate minerals, the most dominant of which are Fe-rich clays.

4. Discussion

Previous interpretations of the magnetic susceptibility records of these Indian Ocean sediments were based on the assumptions that magnetic susceptibility depended on the concentration of ferrimagnetic minerals [e.g., *Clemens and Prell*, 1991] and that the principal factor constraining its use as an indicator of terrigenous input was sediment diagenesis [*deMenocal et al.*, 1991]. Such assumptions raise the apparent paradox that the susceptibility/climate signal is preserved downcore, despite clear evidence of diagenetic destruction of most of the discrete ferrimagnetic grains. *Bloemendal et al.* [1993] resolved the conflict by inferring that sufficient ferrimagnetic grains survived to carry the magnetic susceptibility. The present study demonstrates that, for all but the top ~7 m of the Hole 722 sediments, the susceptibility signal is carried not by ferrimagnetic minerals but by paramagnets. Even within the top ~2 - 7 m, where the coarser ferrimagnetic particles survive, the susceptibility comprises a combination of a paramagnetic and ferrimagnetic signal.

In the upper ~7 m of Hole 722B, a climatic signal is recorded by the ferrimagnetic component, but with a rapid downcore decay in the abundance of these magnetic minerals. Within this interval (0 - 190 ka) the remanence properties vary between glacial and interglacial stages, with larger amounts of ferrimagnetic (submicron to silt- and sand-sized) grains being supplied during glacial stages. This probably reflects an increased supply of eolian dust during glacial periods as a result of increased aridity and/or wind-speed in Somalia and the Arabian Peninsula [*Clemens and Prell*, 1991].

Below ~7 mbsf in Hole 722B, the mineralogical basis for the susceptibility/climate link (i.e., once the effects of carbonate dilution have been removed) is the influx and subsequent preservation of paramagnetic minerals. The abundance of terrigenous Fe-rich clays controls the magnetic susceptibility (below ~7 mbsf) at this site. The clays are less vulnerable to diagenetic modification than the Fe oxides [*Canfield et al.*, 1992]. Hence the paramagnetic susceptibility signal persists, while the record from discrete ferrimagnetic grains is progressively erased.

The carbonate-free susceptibility record of single samples from below ~7 mbsf shows only small-scale variations (Figure 5), but these measurements are influenced by measurement noise because they are relatively close to the detection limit of the susceptibility meter. A higher-resolution record is provided by the whole-core magnetic susceptibility data (Figure 5). However, this volume susceptibility record is influenced both by carbonate dilution and changes in bulk density of the sediment. To obtain the mass susceptibility of the terrigenous component of the sediment, we have used the whole-core magnetic susceptibility, density, carbonate content, and terrigenous percent data tabulated by *Clemens and Prell* [1991], which were measured at ~0.2-m intervals. The mass susceptibility of the terrigenous component (χ_{ter}) is given by

$$\chi_{ter} = 100^* (\chi_{tot} - \chi_{carb})/\%\ \text{terrigenous fraction}, \quad (3)$$

where χ_{tot} is the mass susceptibility of the total sediment (calculated by dividing the whole-core volume susceptibility by the sediment density values of *Clemens and Prell* [1991] and then converting to SI units), and χ_{carb} is the mass susceptibility of the carbonate fraction (determined from the carbonate content and from a susceptibility value for calcite of -0.48×10^{-8} m^3kg^{-1} [*Dunlop and Özdemir*, 1997]). The resulting mass susceptibility record (Figure 14) shows (1) enhancement of the terrigenous mass

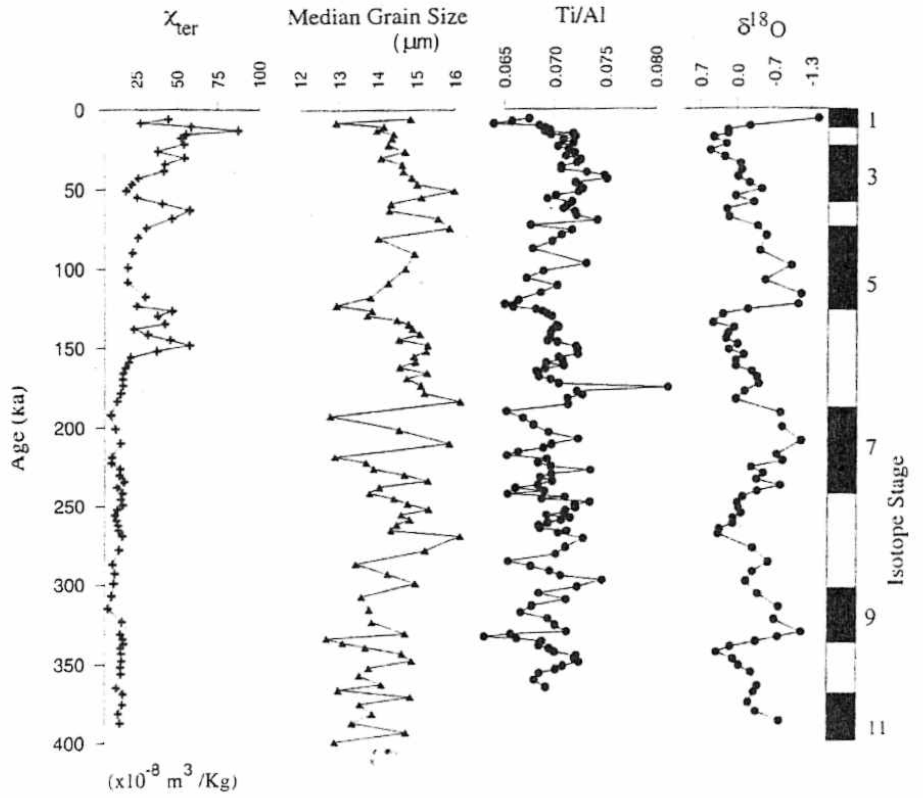

Figure 14. Mass specific susceptibility of the terrigenous fraction (χ_{ter}), with lithogenic grain size [from *Clemens and Prell*, 1991], Ti/Al [from *Shimmield and Mowbray*, 1991], and $\delta^{18}O$ stages [from *Prell et al.*, 1989] also indicated.

susceptibility during glacial stages in the upper ~7 m (0 – 160 ka), (2) additional cyclicity within the upper ~7 m, which is out of phase with the glacial/interglacial oscillations (possibly a reflection of the changing paramagnetic/ferrimagnetic mix), (3) the loss of the glacial/interglacial cyclicity below ~7 mbsf (~ 160 ka), and (4) the higher resolution and precision of the χ_{ter} data (Figure 14) compared with the single-sample mass susceptibility data in Figure 5.

Spectral analysis, using the methods described by *Lomb* [1976], of the terrigenous mass susceptibility record for the interval from 160 ka - 1.4 Ma (i.e., below ~7 mbsf in Hole 722B) enables identification of strong periodicities at 200, 120, 55, 50, 48, 33, 28, 21 and 18 kyr (Figure 15). For a Lomb periodogram, assessment of statistical significance is not straightforward; by definition, the periodogram is based on irregularly spaced data, and accurate assessment of significance requires the removal of each significant cycle as it is identified. However, the labelled peaks are significantly different from what would be expected from a random series. While some of these spectral peaks might possibly be interpreted as near-coincident with the primary Milankovitch periods of 100, 41, 23, and 19 ka, others cannot be related directly to orbital forcing. Notably, the peaks centered near 55, 50, 48, 33, and 28 ka closely match the non-Milankovitch spectral peaks identified by *Clemens and Prell* [1991] for the record of lithogenic grain size in Hole 722B. The lithogenic grain size record shows little correlation with either the terrigenous percent or the sediment accumulation rate [*Clemens and Prell*, 1991]. Conversely, terrigenous percent (Figure 2) (and its inverse, $CaCO_3$ %), the Ti/Al ratio (Figure 14), and whole-core susceptibility are all highly inter-correlated and contain Milankovitch periodicities of 100, 40, and 23 ka [*Shimmield and Mowbray*, 1991]. This suggests that both lithogenic grain size and terrigenous mass susceptibility are decoupled from these other climate indicators and from their orbital forcing mechanisms. That lithogenic grain size and terrigenous mass susceptibility display a lack of correspondence with the Ti/Al ratio may be significant, because Ti/Al ratios are considered to be an indicator of wind strength [e.g., *Shimmield and Mowbray*, 1991]. If grain size and the susceptibility of the terrigenous dust

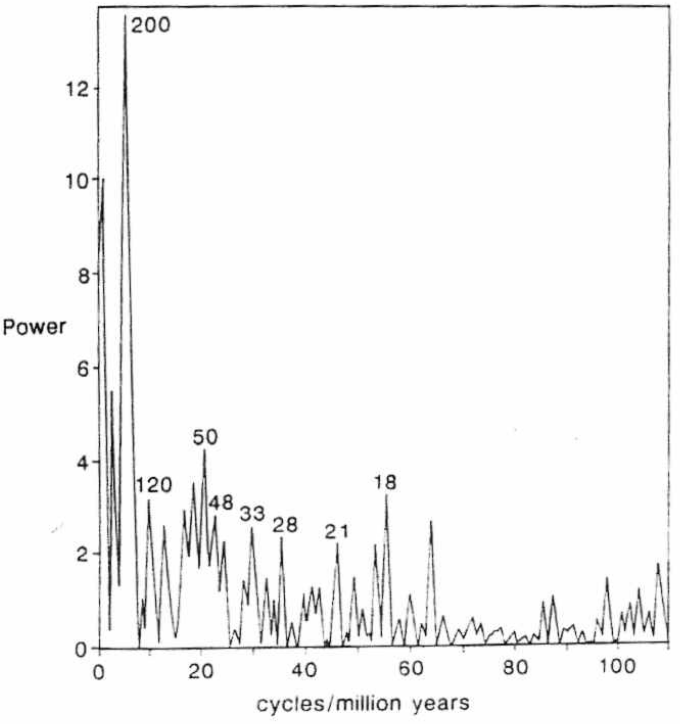

Figure 15. Lomb periodogram for mass specific susceptibility of the terrigenous fraction (χ_{ter}) for the interval from 190 ka to 1.4 Ma. Peaks and spectral power are indicated with periodicities in kyr.

do not reflect variations in wind strength, then they may indicate variations in source of the dust. Hence the grain size and mass susceptibility records may indicate changes in moisture and hence dust supply of different source areas and/or variations in the dust-transporting wind patterns. Such effects appear not to be controlled by monsoon intensity. Site 722 is located in a pivotal position with respect to several major eolian pathways, including summer southwest and northwest monsoon winds and winter northeasterlies (Figure 1). It may be possible to identify these postulated source changes by further mineralogical analyses across the grain size and susceptibility transitions.

5. Conclusions

To understand changes in magnetic susceptibility of sediments in terms of climatic factors, it is necessary to (1) understand the mineralogical source of the magnetic susceptibility, (2) identify the effects of diagenesis on the magnetic record, and (3) examine the response of the individual magnetic components to changes in climatic forcing.

The magnetic susceptibility signal at ODP Hole 722B is primarily controlled not by the abundance of ferrimagnetic minerals, but by the abundance of paramagnetic minerals. The paramagnetic properties are carried by a variety of minerals which dominantly include Fe-rich clays, ilmenite, and other Fe silicates (e.g., amphiboles and pyroxenes). In light of this information, carbonate-free mass susceptibility at this site is an accurate recorder of the abundance of the detrital Fe-bearing silicate fraction.

Diagenesis has had a major impact in modifying the detrital ferrimagnetic record at Hole 722B. The downcore rate of destruction of the remanence-bearing minerals is exponential over the first ~7 m, below which the dissolution continues but at a slower rate. Below ~7 mbsf, ferrimagnetic inclusions play an increasing role in determining the magnetic remanence properties of the sediment.

Climatic information carried by the ferrimagnetic signal is seen only in the sediment that has not undergone extensive diagenetic dissolution, i.e., the top ~7 m of Hole 722B. In this interval, there is strong glacial/interglacial control of the magnetic properties, with larger amounts of ferrimagnetic material being supplied during glacial stages. The most likely paleoenvironmental control on these magnetic shifts is enhanced continental aridity during glacial periods, which supplies these sediments with increased concentrations of lithogenic detrital magnetite. It is possible that production of bacterial magnetite is enhanced during interglacial stages, as a response to changes in the microenvironment (e.g., oxygen and nutrient content) in the bottom waters and near the sediment/water interface. The contribution of bacterial magnetosomes to the magnetization of the Hole 722B sediments is, however, very small.

The paramagnetic susceptibility record responds at a different frequency to the ferrimagnetic record, i.e., at a frequency that also reflects changes in the lithogenic grain size. Both the grain size and paramagnetic susceptibility records are decoupled from the lithogenic percent, carbonate percent, sediment accumulation rate and the Ti/Al ratio. If the latter represents a proxy for wind strength, then the grain size and susceptibility records may indicate changing dust source areas.

In summary, for Hole 722B, the magnetic responses to climate change include the following: (1) fluctuations in the bulk volume magnetic susceptibility, which are primarily controlled by carbonate dilution (hence the response is largely controlled by carbonate productivity and the amount of dust arriving at the site); (2) a ferrimagnetic signal only within the upper ~7 m, which largely reflects aridity in the source area, that is in turn controlled by fluctuations in ice volume; and (3) a paramagnetic susceptibility record below ~7 mbsf, which coincides in frequency with lithogenic grain size.

Acknowledgments. This work was supported by a research grant to B.A.M. from the NERC, UK. The time series analysis was performed by Mick Kelly, Climatic Research Unit, University of East Anglia. Some of the XRD analyses were carried out at the Institute for Food Research, Norwich, England. Graham Shimmield kindly provided the XRF data for determination of carbonate contents.

References

Bloemendal, J., Paleoenvironmental implications of the magnetic characteristics of sediments from Deep-Sea Drilling Project Site 514, southeast Argentine Basin, *Init. Rep. Deep Sea Drill. Proj., 71*, 1097-1108, 1983.

Bloemendal, J., and P. deMenocal, Evidence for a change in the periodicity of tropical climate cycles at 2.4 Myr from whole-core magnetic susceptibility measurements, *Nature, 342*, 897-900, 1989.

Bloemendal, J., J.W. King, A. Hunt, P.B. deMenocal, and A. Hayashida, Origin of the sedimentary magnetic record at the Ocean Drilling Program sites on the Owen Ridge, western Arabian Sea, *J. Geophys. Res., 98*, 4199-4219, 1993.

Brindley, G.W., Quantitative X-ray mineral analysis of clays, in *Crystal Structures of Clay Minerals and Their X-Ray Identification*, (edited by G.W. Brindley and G. Brown), pp.411-438, Mineral. Soc., London, 1980.

Canfield, D.E., and R.A. Berner, Dissolution and pyritization of magnetite in anoxic marine sediments, *Geochim. Cosmochim. Acta, 51*, 645-659, 1987.

Canfield, D.E., R. Raiswell, and S. Bottrell, The reactivity of sedimentary iron minerals towards sulfide, *Am. J. Sci., 292*, 659-683, 1992.

Clemens, S.C., and W.L. Prell, One million year record of summer monsoon winds and continental aridity from the Owen Ridge (Site 722), northwest Arabian Sea, *Proc. Ocean Drill. Program Sci. Results, 117*, 365-388, 1991.

deMenocal, P., J. Bloemendal, and J. King, A rock magnetic record of monsoonal dust deposition to the Arabian Sea: Evidence for a shift in the mode of deposition at 2.4 Ma, *Proc. Ocean Drill. Program Sci. Results, 117*, 389-407, 1991.

Dimanche, F., and P. Bartholome, The alteration of ilmenite in sediments, *Miner. Sci. Eng., 8*, 187-201, 1976.

Dunlop, D., and K. Argyle, Thermoremanence, anhysteretic remanence, and susceptibility of submicron magnetites: Nonlinear field dependence and variation with grain size, *J. Geophys. Res., 102*, 20,199-20,210, 1997.

Dunlop, D.J. and Ö. Özdemir, *Rock Magnetism: Fundamentals and Frontiers*, Cambridge Univ. Press, New York, 1997.

Heller, F., C.D. Shen, J. Beer, X.M. Liu, T.S. Liu, A. Bronger, M. Suter, and G. Bonani, Quantitative estimates of pedogenic ferromagnetic mineral formation in Chinese loess and paleoclimatic implications, *Earth Planet. Sci. Lett., 114*, 385-390, 1993.

Hooten, D.H., and N.E. Giorgetta, Quantitative X-ray diffraction analysis by a direct calculation method, *X Ray Spectrometry, 6*, 2-5, 1977.

Hounslow, M.W., and B.A. Maher, Quantitative extraction and analysis of carriers of magnetisation in sediments, *Geophys. J. Int., 124*, 57-74, 1996.

Hounslow, M.W., and B.A. Maher, Laboratory procedures for quantitative extraction and analysis of magnetic minerals from sediments, in *Environmental Magnetism: A Practical Guide*, edited by J. Walden, F. Oldfield, and J.P. Smith, Quat. Res. Assoc., Cambridge, England, pp.139-184, 1999.

Keefer, C.M., and P.N. Shive, Curie temperature and lattice constant reference contours for synthetic titanomagnetite, *J. Geophys. Res., 86*, 987-998, 1981.

Lomb, N.R., Least-squares frequency analysis of unequally spaced data, *Astrophys. Space Sci., 39*, 447-462, 1976.

Maher, B.A., Magnetic properties of modern soils and Quaternary loessic

paleosols: Paleoclimatic implications, *Palaeogeog., Palaeoclimatol., Palaeoecol., 137*, 25-54, 1998.

Maher, B.A., Magnetic properties of some synthetic sub-micron magnetites, *Geophys. J. R. Astron. Soc., 94*, 83-96, 1988.

Maher, B.A., R. Thompson, and L.P. Zhou, Spatial and temporal reconstructions of changes in the Asian paleomonsoon: A new mineral magnetic approach, *Earth Planet. Sci. Lett., 125*, 461-471, 1994.

Morad, S., and A.A. Aldahan, Alteration of detrital Fe-Ti oxides in sedimentary rocks, *Geol. Soc. Am. Bull., 97*, 567-578, 1986.

Özdemir, Ö., and S.K. Banerjee, A preliminary magnetic study of soil samples from west-central Minnesota, *Earth Planet. Sci. Lett., 59*, 393-403, 1982.

Pedersen, T.F., and G.B. Shimmield, Interstitial water chemistry, Leg 117: Contrasts with the Peru Margin, *Proc. Ocean Drill. Program, Sci. Results, 117*, 499-516, 1991.

Prell, W.L., N. Niitsuma, et al., Site 722, *Proc. Ocean Drill Program Init. Rep., 117*, 255-318, 1989.

Qasim, S.Z., Oceanography of the northern Arabian Sea, *Deep Sea Res., Part A, 29*, 1041-1068, 1982.

Richter, C., and B.A. van der Pluijm, Separation of paramagnetic and ferrimagnetic susceptibility using low temperature magnetic susceptibility and comparison with high field methods, *Phys. Earth Planet. Inter., 82*, 113-127, 1994.

Righi, D., and P. Jadualt, Improving soil clay mineral studies by high gradient magnetic separation, *Clay Miner., 23*, 225-232, 1988.

Robinson, S.G., Applications for whole-core susceptibility measurements of deep-sea sediments: ODP Leg 115 results, in Duncan, R.A., J. Backman, L.C. Peterson, et al., *Proc. Ocean Drill. Program Sci. Results, 115*, 737-771, 1990.

Robinson, S.G., M.A. Maslin, and I.N. McCave, Magnetic-susceptibility variations in upper Pleistocene deep-sea sediments of the NE Atlantic-Implications for ice rafting and paleocirculation at the last glacial maximum, *Paleoceanography, 10*, 221-250, 1995.

Rochette, P., and G. Fillion, Identification of multicomponent anisotropies in rocks using various field and temperature values in a cryogenic magnetometer, *Phys. Earth Planet. Inter., 51*, 379-386, 1988.

Shackleton, N.J., et al., Oxygen isotope calibration of the onset of ice-rafting in DSDP site 552A: A history of glaciation in the North Atlantic region, *Nature, 335*, 708-711, 1984.

Shimmield, G.B., and S.R. Mowbray, The inorganic geochemical record of the Southwest Arabian Sea: A history of productivity variation over the last 400 ky from Sites 722 and 724, *Proc. Ocean Drill. Program Sci. Results, 117*, 409-430, 1991.

Shimmield, G.B., S.R. Mowbray, and G.P. Weedon, A 350 ka history of the Indian Southwest monsoon--Evidence from deep-sea cores, *Trans. R. Soc. Edinburgh Earth Sci., 81*, 289-299, 1990.

Sun, W., and M.J. Jackson, Scanning electron microscopy and rock magnetic studies of magnetic carriers in remagnetized early Paleozoic carbonates from Missouri, *J. Geophys. Res., 99*, 2935-2942, 1994.

Thompson, R., and F. Oldfield, *Environmental Magnetism*, Allen and Unwin, London, 1986.

von Dobeneck, T., Gesteinmagnetische Untersuschungen an tiefseesedimenten des Sudatlantiks, Diplomarbeit, 128 pp., Inst. für Allg. Angew. Geophys., Ludwig-Maximilians-Univ., Munich, Germany, 1985.

Weedon, G.P., and G.B. Shimmield, Late Pleistocene upwelling and productivity variations in the northwest Indian Ocean deduced from spectral analyses of geochemical data from Sites 722 and 724, *Proc. Ocean Drill. Program Sci. Results, 117*, 431-443, 1991.

M. W. Hounslow and B. A. Maher, School of Environmental Sciences, University of East Anglia, Norwich NR4 7TJ, England, United Kingdom. (*m.hounslow@uea.ac.uk; b.maher@uea.ac.uk*)

(Received May 8, 1998; revised August 17, 1998;
accepted November 10, 1998.)